Improved Performance of P3HT:PCBM-Based Solar Cells Using Nematic Liquid Crystals as a Processing Additive under Low Processing Temperature conditions[a]

Soo Won Heo, Kyeong Hun Baek, Ho Jun Song, Tae Ho Lee, Doo Kyung Moon*

Nematic liquid crystals (NLCs) are introduced to P3HT:PCBM-based bulk heterojunction polymer solar cells (PSCs) as processing additives for low processing temperatures. To investigate why the addition of NLCs improves the efficiency of PSCs, the photon absorbance properties are observed using UV–vis spectroscopy and photoluminescence. Then, the degree of crystallinity of P3HT is examined through X-ray diffraction analysis. In addition, changes in the nanostructure and surface morphology of the P3HT:PCBM blend film are observed through atomic force microscopy and transmission electron microscopy.

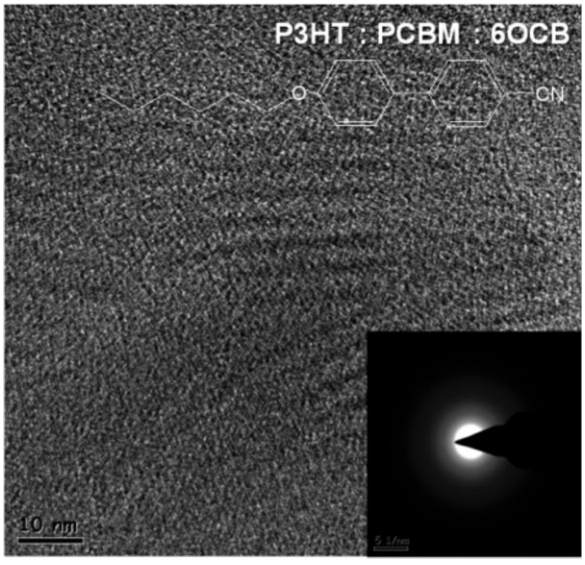

1. Introduction

π-Conjugated polymer-based polymer solar cells (PSCs) offer the advantage of easy fabrication of light-weight devices with superior mechanical properties.[1–3] Therefore, if spin-coating, ink-jet printing, roll-to-roll printing, brush painting, or stamping techniques are applied to the flexible substrate, light-weight, and flexible, large-area photovoltaic devices can be fabricated inexpensively.[4–9]

More than a decade of development has improved the maximum power conversion efficiency (PCE) of PSCs to about 7–8%.[10–12] Therefore, many studies have been conducted on the design of new low band-gap polymer materials in order to improve PCE,[13,14] improvement in the understanding of bulk heterojunction (BHJ) device physics[15] and develop novel device fabrication methods and structures.[16–18]

BHJ PSCs are applied to the photoactive layer after blending an electron-donating material (p-type conjugated polymers) with an electron-accepting material (n-type fullerene derivatives). To improve the PCE of BHJ PSCs, continuous pathways must be formed to allow excited electrons and holes to be transferred to the external circuit without recombining with each other. The typical BHJ PSCs comprise a system of poly (3-hexylthiophene-2,5-diyl) (P3HT) as an electron donor and [6,6]-phenyl-C_{61}-butyric acid methyl ester (PCBM) as an electron acceptor. In this

Dr. S. W. Heo, K. H. Baek, Dr. H. J. Song, T. H. Lee, Prof. D. K. Moon
Department of Materials Chemistry and Engineering, Konkuk University, 1 Hwayang-dong, Gwangjin-gu Seoul 143-701, Korea
E-mail: dkmoon@konkuk.ac.kr

[a]**Supporting Information** is available from the Wiley Online Library or from the author.

DOI: 10.1002/mame.201300168

system, PCBM is dispersed among the P3HT chains and prevents P3HT from being crystallized. Therefore, untreated BHJ PSCs have low PCE under 1%.[19] In order to improve the PCE of P3HT/PCBM BHJ PSCs, therefore, P3HT and PCBM should exist in an interpenetrating network form and should be very well phase-separated. In several groups, the efficiency has been improved by thermally annealing of the BHJ films to form a well-defined bicontinuous interpenetrating network between P3HT and PCBM.[20] Vanlaeke et al.[19] and Padinger et al.[21] achieved a PCE of 2–3% by using thermal annealing to improve the morphology of the BHJ film. Ma et al.[22] also improved PCE up to ca. 5.1% through post-thermal annealing at 150 °C. When the post-thermal annealing temperature is not appropriately controlled, however, thermal annealing at high temperature after deposition of the cathode can cause damage to the morphology of the BHJ films. Also, this additional annealing process consumes a lot of time for fabrication of PSCs. Moreover, the flexible plastic substrates for PSCs are not capable of withstanding the high annealing temperature because they have low glass transition temperatures (T_g) (PET; $T_g = 78$ °C and PEN; $T_g = 121$ °C).

To increase the device performances at low device fabrication temperature, many groups were introduced a solvent treatment method for controlling the physical behavior of the polymer blend. Li et al. improved PCE by controlling the solvent evaporation rate and film growth rate. This solvent annealing method improved the ordered structure formation of P3HT in the film by offering more time to help the P3HT chains to continue their self-organization process before the P3HT/PCBM solution was turned into a solid film.[23] In addition, Zhang et al.[24] introduced a "solvent mixing method" which blended two organic solvents with different boiling point. Even though the P3HT chain was reorganized by introducing a solvent mixture to which a small amount of chlorobenzene (CB; b.p. 132 °C) had been added to the host solvent chloroform (b.p. 61 °C), a low PCE of 2.3% was observed. Studies have also been reported on BHJ PSCs with performance enhanced by adding a few volume percent of processing additives (e.g., 1,8-diiodooctane, 1,8-octanedithiol, and 1-bromonaphthalene) to the host solvent in a similar method.[20,25,26] These processing additives can improve the degree of crystallinity of the polymer by nanoscale phase-separation of the polymer and PCBM. However, most known processing additives have been applied to the cases in which a low band-gap polymer has been used as an electron donor material. In the P3HT/PCBM system, alkanethiols such as 1,8-octanedithiol have been used to decrease the degree of crystallinity of P3HT because they have an impact on the nanoscale phase separation of P3HT/PCBM by aggregating P3HT.

In general, liquid crystals (LCs) such as discotic columnar, smectic, and nematic LCs have the potential to become an important class of charge mobility materials.[27] Among them, smetic liquid crystals (SLCs) and nematic liquid crystals (NLCs) have many advantages include spontaneous self-assembly, relatively high charge mobility (1×10^{-3} $cm^2 V^{-1} s^{-1}$) and easy film formation by spin coating, slot-die coating, or ink-jet printing.[28]

In this study, therefore, NLCs such as 4′-(pentyloxy)-4-biphenylcarbonitrile (5OCB), 4′-(hexyloxy)-4-biphenylcarbonitrile (6OCB), and 4′-(heptyloxy)-4-biphenylcarbonitrile (7OCB) were introduced to P3HT:PCBM-based BHJ PSCs as processing additives for low temperature process and increase the PCE of PSCs by increasing of short circuit current density (J_{SC}) via improving the degree of crystallinity and photon absorption property of the BHJ film. The mechanism of this improvement in the properties of BHJ PSCs is determined by observing the optical, electrical, and structural properties of the BHJ film after adding the processing additives. Using UV/photoluminescence (PL) spectroscopy, the absorption of photons and the quenching properties of the excited electrons were observed. The structural properties of P3HT crystallite were analyzed through X-ray diffraction (XRD) pattern analysis. The phase segregation of the P3HT/PCBM film and the increase of crystallinity in P3HT were observed by atomic force microscopy (AFM) and transmission electron microscopy (TEM) analysis.

2. Experimental Section

2.1. Materials

The indium tin oxide (ITO) glass that was used as the transparent electrode is a Samsung Corning product (ITO: 170 nm, 10 Ω sq^{-1}). Poly(3,4-ethylenedioxythiophene)/poly(styrenesulfonate) (PEDOT:PSS, AI 4083) was purchased from Clevios and P3HT, which was used as a donor material in the photoactive layer, was purchased from Rieke metal. PCBM, the acceptor material, was purchased from Nano C. 1,2-dichlorobenzene (ODCB), which was used as a host solvent, and 5OCB, 6OCB, and 7OCB, which were used as processing additives, were purchased from Aldrich. The chemical structure of P3HT, PCBM are shown in Figure 1a and b. In addition, the chemical structure and phase transition temperature of NLCs are show in Figure 1c.

2.2. Measurements

All of the thin films were fabricated using a GMC2 spin coater (Gensys), and their thicknesses were measured using an alpha step 500 surface profiler (KLA-Tencor). The photon absorption property and quenching property of the excited electrons in the BHJ film were measured with UV–vis spectroscopy (HP Agilent 8453) and PL spectroscopy (Perkin Elmer LS 55 luminescence spectrometer), respectively. The XRD patterns were observed using a Rigaku D/MAX 2200 diffractometer with Cu Kα radiation to confirm the crystalline size of P3HT. The morphology of the BHJ films was

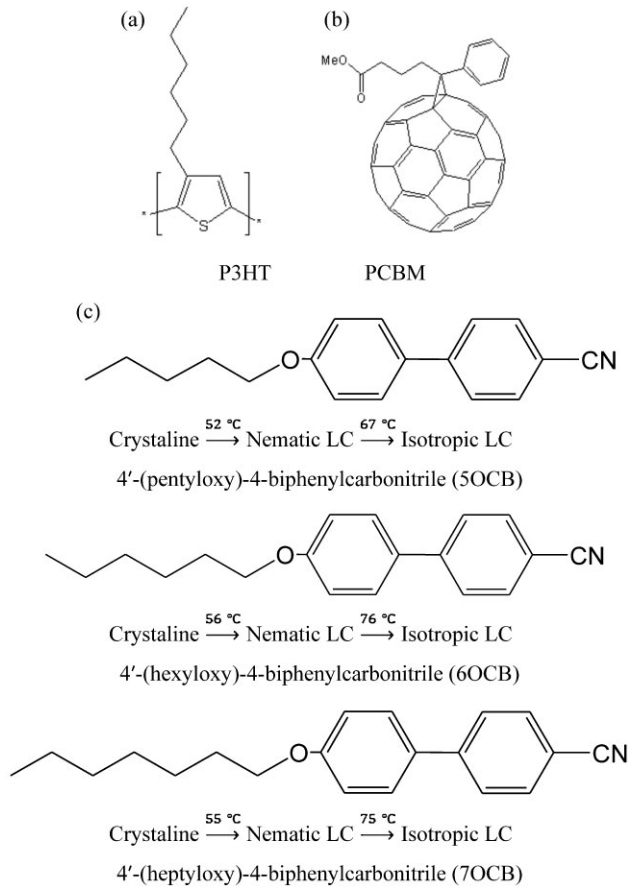

Figure 1. The chemical structure of a) P3HT, b) PCBM. The chemical structure and phase transition temperatures of c) nematic liquid crystals (NLCs).

observed through AFM (PSIA XE-100) and FE-TEM (FEI Tecnai G2 F30), respectively. The surface energy was measured with a contact-angle meter (KRUSS K6). The current density–voltage (*J–V*) characteristics of the PSCs were measured using a Keithley 2400 source measure unit. The devices were evaluated at 298 K by using a Class A Oriel solar simulator (Oriel 96000 150 W solar simulator) having an xenon lamp that simulates AM 1.5G irradiation (100 mw cm^{-2}) from 400 to 1 100 nm. The instrument was calibrated with a monocrystalline Si diode fitted with a KG5 filter to bring the spectral mismatch to unity. The calibration standard was calibrated by the National Renewable Energy Laboratory (NREL). The incident photon to current efficiency (IPCE) was evaluated using Mc Science IPCE measurement system.

2.3. Cleaning of Patterned ITO Glass

To clean the patterned ITO glass, it was sonicated for 20 min. in each of detergent (Alconox in deionized water, 10%), acetone, isopropyl alcohol and deionized water in order. The moisture was removed by blowing thoroughly with N_2 gas. To ensure complete removal of all of the remaining water, the patterned ITO glass was baked on a hot plate for 10 min at 100 °C. For hydrophilic treatment of the patterned ITO glass, it was cleaned for 10 min in a UVO cleaner.

2.4. Fabrication of PSCs

PEDOT:PSS was spin coated from aqueous solution to form a 40-nm-thick film on the patterned ITO glass. The substrate was dried for 20 min at 120 °C in air and then transferred into a glovebox to spin coat the active layer. A solution containing a mixture of P3HT/PCBM (1:0.6) in ODCB with or without various concentrations of NLCs (5OCB, 6OCB, and 7OCB) was then spin coated on top of the PEDOT:PSS layer to give a 130-nm-thick photoactive layer that was then thermal annealing at 50–80 °C for 10–60 min. To form the cathode, BaF_2 (0.1 Å s^{-1}, 2 nm), Ba (0.2 Å s^{-1}, 2 nm) and Al (5 Å s^{-1}, 100 nm) were thermally deposited in order in a high-vacuum chamber. Finally, PSCs with an active area of 4 mm^2 (2 mm × 2 mm) were fabricated through encapsulation.

3. Results and Discussion

Figure 2 shows the *J–V* curve and external quantum efficiency (EQE) when NLCs were added as processing

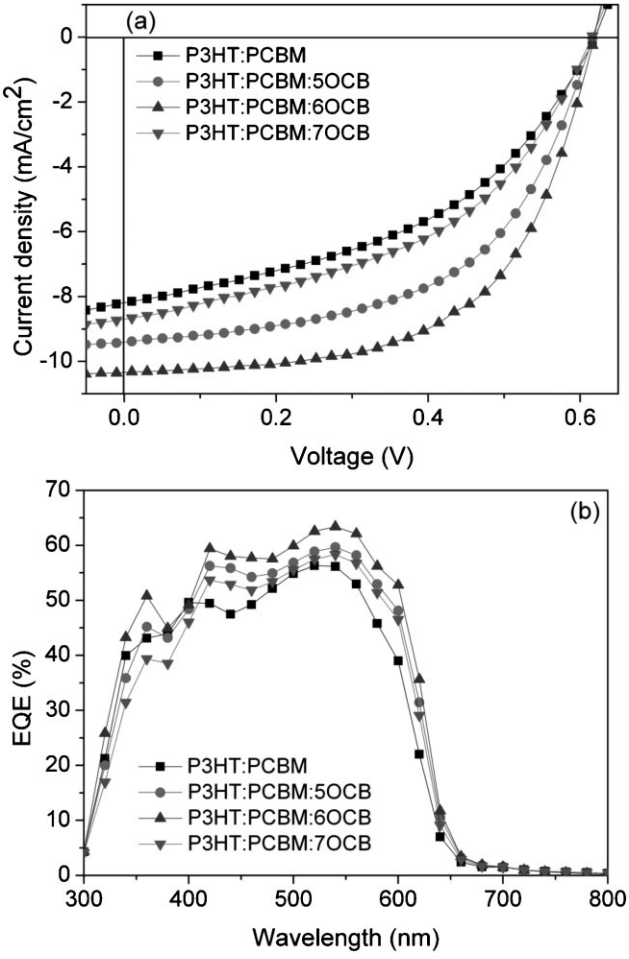

Figure 2. a) *J–V* characteristics and b) external quantum efficiency (EQE) characteristics of P3HT:PCBM = 1:0.6 composite films with various NLCs.

Table 1. Photovoltaic performances of BHJ PSCs composed P3HT:PCBM fabricated with various NLCs.

Processing additive	J_{SC} [mA cm^{-2}]	V_{OC} [V]	FF [%]	PCE [%]	R_S [Ω cm^{-2}]	R_{SH} [Ω cm^{-2}]
None	8.1	0.616	44.9	2.3	23.38	245
5OCB	9.4	0.616	54.6	3.2	13.31	460
6OCB	10.3	0.616	63.0	4.0	9.23	980
7OCB	8.7	0.616	46.3	2.5	18.61	280

ITO(170 nm)/PEDOT:PSS(40 nm)/P3HT:PCBM:NLCs(130 nm)/BaF_2(2 nm)/Ba(2 nm)/Al(100 nm).

additives, and the results are summarized in Table 1. The optimized concentration of the NLCs, annealing temperature, and annealing time were 3 wt%, 70 °C, and 40 min, respectively (see Supporting Information). When 6OCB was added as the processing additive, the open circuit voltage (V_{OC}), short circuit current density (J_{SC}), and fill factor (FF) were 0.616 V, 10.3 mA cm^{-2} and 63.0%, respectively. The calculated PCE of 4.0% was increased by 74% compared to the pristine P3HT based device. Here, the EQE maximum value was 64% at 550 nm. In addition, the PCE of the device with 5OCB was 3.2%, which was increased by 39%. However, the PCE of the device with 7OCB was 2.5%, which was slightly more efficient than the reference. In the devices with an improved efficiency due to the addition of a processing additive, both J_{SC} and FF improved, compared to the reference, but V_{OC} remained unchanged. To investigate the causes of these results, the series resistance (R_S) and shunt resistance (R_{SH}) were measured in each device (Table 1). When 6OCB was added, R_S was 9.23 Ω cm^{-2}, which was decreased by about 2.5-fold compared to the reference (23.38 Ω cm^{-2}). In addition, R_{SH} was 980 Ω cm^{-2}, which was increased by fourfold compared to the reference (245 Ω cm^{-2}). Therefore, the addition of 6OCB increased both J_{SC} and FF.[9] These patterns were also observed in the devices to which 5OCB and 7OCB were added because these three different processing additives which were added to the photoactive layer changed its photon absorption, bicontinuous interpenetrating network, and surface morphology.

Figure 3 shows the photon absorption properties with the addition of NLCs, which were observed using UV–vis spectroscopy. Figure 3a is the UV–vis spectrum of the device in which 5OCB, 6OCB, and 7OCB (3 wt%) were added to the P3HT film as processing additives. When 5OCB, 6OCB, and 7OCB were added to P3HT, the photon absorption properties were increased compared to the pristine P3HT film. Moreover, maximum absorption peak (λ_{max}) values were red-shifted from 505 to 521 nm because of the π–π^* transition among the P3HT molecules.[29] This suggested that the crystallinity was improved compared to that of the pristine P3HT:PCBM film. Figure 3b shows the UV–vis spectrum of the device in which 5OCB, 6OCB, and 7OCB (3 wt%) were added to the P3HT:PCBM blended film as processing additives. When 6OCB was added, in particular, an increase in absorbance over the wavelength range from 450 to 600 nm because of π–π transition among P3HT molecules was observed.[20,30] It contributes to the increase in the PCE compared to the pristine device.

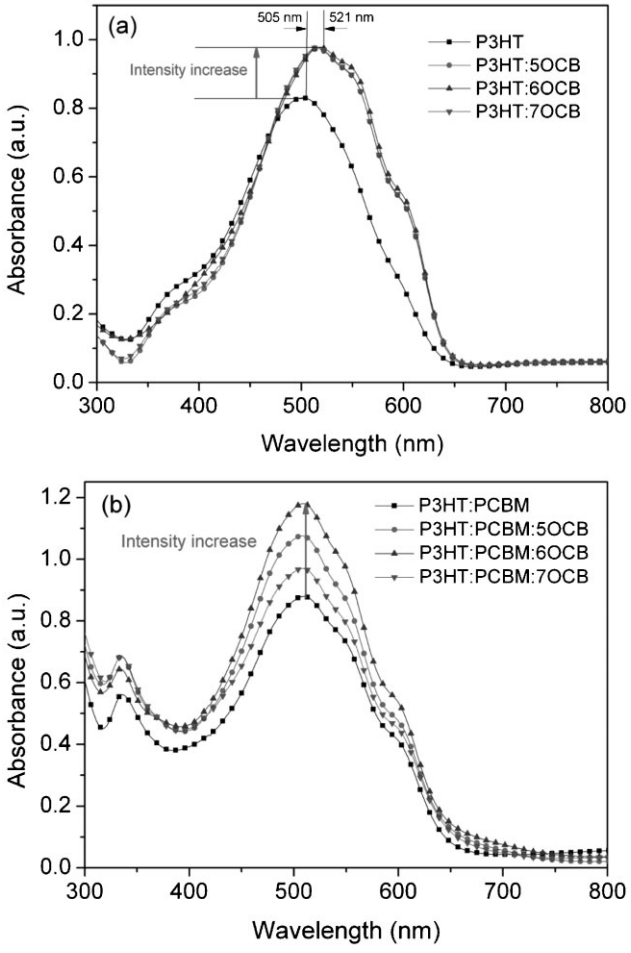

Figure 3. UV–vis absorption spectra of a) P3HT films with/without NLSc, b) P3HT:PCBM blending films with/without NLCs.

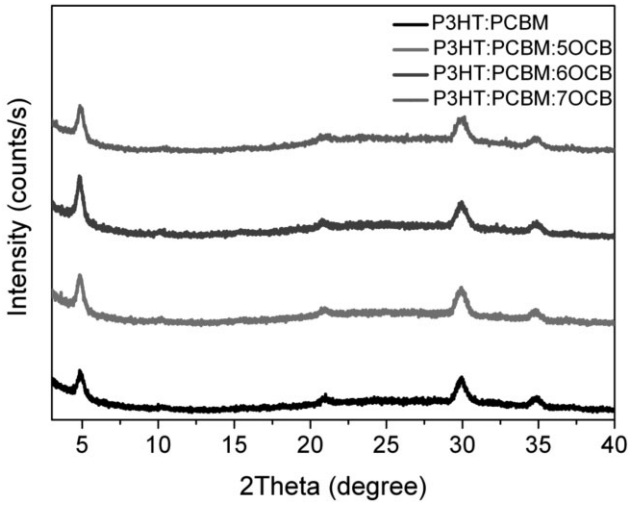

Figure 4. X-ray diffraction pattern of P3HT:PCBM blend films with and without NLCs.

To investigate the ordering of the P3HT chain induced by the addition of the NLCs, the XRD pattern is shown in Figure 4. The intensity of the (100) diffraction peak was increased at $2\theta = 4.8^{\circ}$ in the film to which 5OCB, 6OCB, and 7OCB were added, compared to the P3HT:PCBM blended film. The peaks at $2\theta = 22^{\circ}$, 31°, and 35° arises from ITO. An ordered lamellar structure with an interlayer spacing originating from the interdigitated alkyl chains of P3HT was observed in the annealed films.[19] Moreover, the increased intensity indicated an increased crystallinity in P3HT, and hence that the NLCs affected the bicontinuous interpenetrating network of P3HT and PCBM. As a result, the crystallinity of P3HT increased. The crystalline size of P3HT was calculated by using the following Scherrer's equation: $(L = K\lambda\lambda/B\cos\theta)$, where L is the average crystalline size of P3HT (100), B the full width at half maximum (FWHM) of (100) peak, λ the wavelength of the incident X-rays (0.154 nm), θ the angle of refraction, and K Scherrer's constant (0.9). Based on Scherrer's equation, the crystalline size of each P3HT is stated in Table 2. In P3HT, to which no NLC had been added, the crystalline size was about 16 nm.

Table 2. Crystalline size of P3HT.

Processing additives	Crystalline size of P3HT [nm]
None	16
5OCB	23
6OCB	29
7OCB	21

However, it gradually increased when 6OCB were added. The addition of 6OCB increased the size up to 29 nm. This increase of P3HT crystalline size was attributed to the improved carrier mobility that was created in the photoactive layer. Consequently, J_{SC} and FF of PSCs were improved and, therefore, calculated PCE was also improved.

After fabricating a hole-only device for a charge mobility study, the hole mobilities were calculated using the SCLC.[31] The configuration of hole-only devices was ITO/PEDOT:PSS/photo active layer/MoO_3/Al. The reference device exhibited a hole mobility of $5.60 \times 10^{-4}\,cm^2 \cdot V^{-1}\,s^{-1}$. The device in which 6OCB was doped to the photoactive layer had a hole mobility of $3.14 \times 10^{-3}\,cm^2 \cdot V^{-1}\,s^{-1}$, which indicated that 6OCB improved carrier mobility. This result confirmed that processing additives doping improved the photon-harvesting properties in the photoactive layers and also enhanced the hole mobility. Furthermore, processing additives were able to send the generated holes to the external circuit quickly without recombination.

Figure 5 shows the PL quenching in order to determine whether the excitons that were generated on the photoactive layer were efficiently dissociated. The difference between the areas of the graph in which the acceptor PCBM was and was not included represents a quenched electron hole. As the quenched amount increases, the efficiency of electron–hole dissociation improves. As shown in Table 3, 67% of the quenching ratio was observed in P3HT, in which no processing additives had been added to the photoactive layer. In comparison, 93, 88, and 82% of quenched ratio were detected when 6OCB, 5OCB, and 7OCB were added, respectively, indicating a maximum increase of 38% for 6OCB. These quenched ratios were all greater than that of P3HT. Therefore, the addition of NLCs improved the

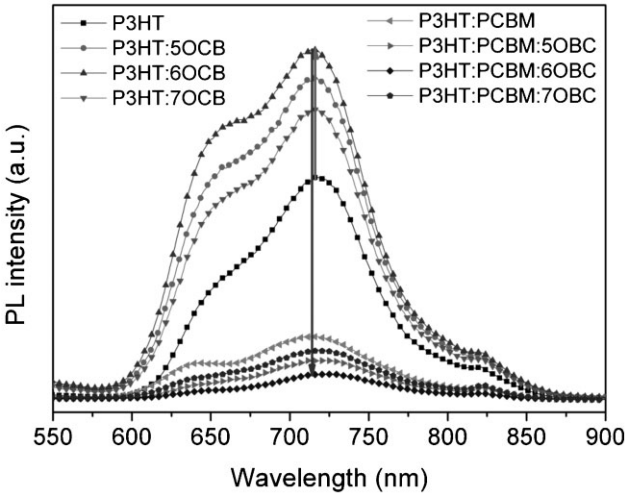

Figure 5. PL quenching data of P3HT films with/without NLCs and P3HT:PCBM blend films with/without NLCs.

Table 3. Calculated PL quenching area.

Processing additive	Quenching area [%]
None	67
5OCB	88
6OCB	93
7OCB	82

absorption properties by causing π–π^* transition among the P3HT molecules and promoted carrier mobility by increasing crystallinity in P3HT. Therefore, the ability to absorb more photons without the NLCs allowed them to be quickly transferred to the external circuit without having to prevent them from being recombined. To investigate the effect of the processing additives on the structural properties of the BHJ-structured photoactive layer, they were analyzed through AFM and TEM. Figure 6 shows the changes as observed through AFM in the surface morphology induced by with/without NLC and its type in the P3HT:PCBM films. The root mean square (RMS) roughness of the device to which 6OCB had been added (0.54 nm) was lower than that of the device without any NLCs (0.64 nm). This confirmed that the addition of 6OCB improved the P3HT–PCBM phase separation, leading to the formation of a nanoscale domain. In addition, because the NLCs such as 6OCB have a spontaneous self-assembly property, can be reorganization of P3HT chains to improve the carrier mobility. The addition of NLCs allowed the nanoscale domain to provide a pathway through which holes and electrons that had been separated after forming an interpenetrating network could be transferred to the

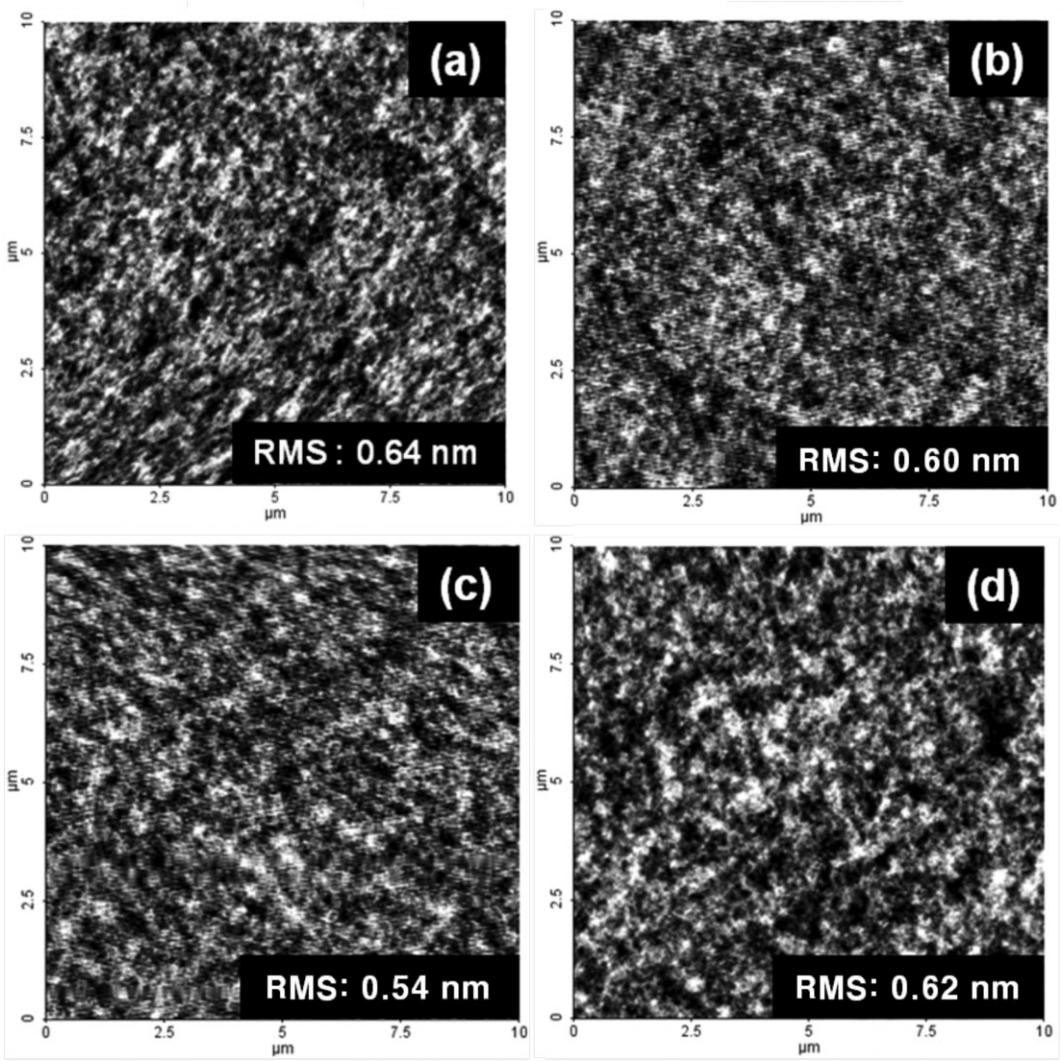

Figure 6. AFM image of films cast from P3HT:PCBM with/without NLCs. a) P3HT:PCBM, b) 5OCB, c) 6OCB, and d) 7OCB.

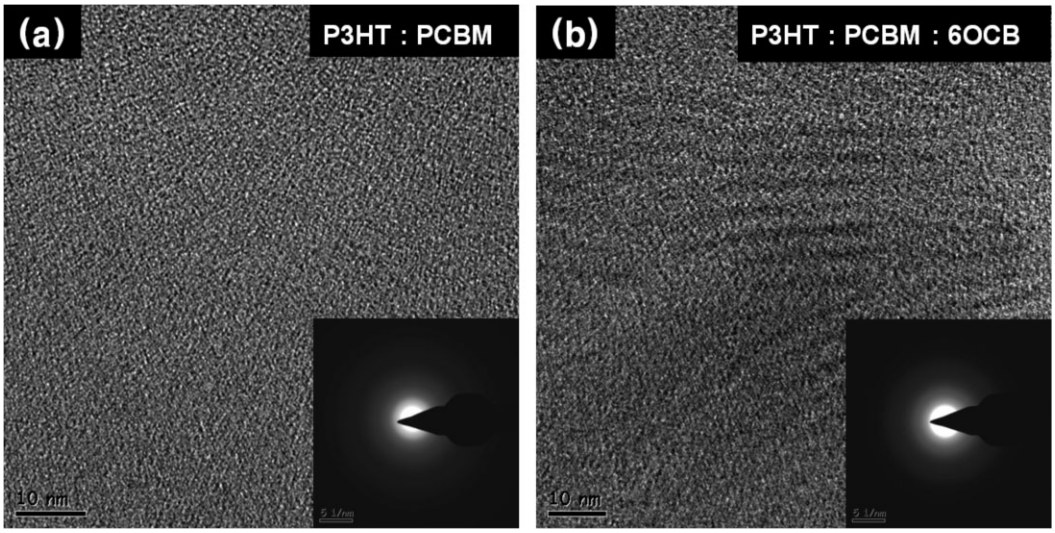

Figure 7. TEM image of films cast from P3HT:PCBM a) without NLCs (inset: SAED pattern) and b) with 6OCB (inset: SAED pattern).

cathode, increase J_{SC}, and prevent them from being recombined while the carrier is on the move. Therefore, R_S decreased while R_{SH} increased in the devices to which any NLCs had been added. As a result, both J_{SC} and FF were improved.

Figure 7 shows TEM images of a thin film in which 3 wt% of 6OCB had been added to P3HT:PCBM and P3HT:PCBM. As shown in Figure 7b, fingerprint texture was observed. This confirmed that P3HT was reorganized by added 6OCB in P3HT:PCBM blend because the NLC has a self-assembling property.[29] Therefore, from the selected area electron diffraction (SAED) pattern shown in Figure 7b inset, the addition of 6OCB improved the crystallinity in P3HT. It was concluded that a nanoscale domain can be formed through the addition of NLCs, and that the separated holes and electrons can be effectively dissociated through large-scale phase separation. Furthermore, the carriers were shown to be quickly transferred because of the polymer crystallinity at low processing temperature.

4. Conclusion

In summary, we dramatically improved the efficiency of fabricated P3HT:PCBM-based PSCs by adding NLCs as processing additives at low processing temperature. The addition of these NLCs improved the degree of crystallinity of P3HT. In addition, the formation of a nanoscale domain and interpenetrating network enabled has made it possible for a carrier to move quickly to the external circuit, and the absorbance was improved by the resulting increase in photon harvesting properties. As a result, R_S decreased while R_{SH} increased. Finally, PCE was improved by 74% due to the increase in J_{SC} and FF.

Acknowledgments: This research was supported by a grant (10037195) from the Fundamental R&D Program for Core Technology of Materials funded by the Ministry of Knowledge Economy, Republic of Korea and the National Research Foundation of Korea Grant funded by the Korean Government(MEST) (NRF-2009-C1AAA001-2009-0093526).

Received: April 23, 2013; Revised: May 29, 2013; Published online: July 11, 2013; DOI: 10.1002/mame.201300168

Keywords: carrier mobility; low-processing temperature; nematic liquid crystals; polymer solar cells; processing additives

[1] H.-Y. Chen, J. H. Hou, S. Q. Zhang, Y. Y. Liang, G. W. Yang, Y. Yang, L. P. Yu, Y. Wu, G. Li, *Nat. Photonics* **2009**, *3*, 649.
[2] Y. Liang, Z. Xu, J. Xia, S.-T. Tsai, Y. Wu, G. Li, C. Ray, L. Yu, *Adv. Mater.* **2010**, *22*, E135.
[3] J. Y. Lee, Y. J. Kwon, J. W. Woo, D. K. Moon, *J. Ind. Eng. Chem.* **2008**, *14*, 810.
[4] F. C. Krebs, *Sol. Energy Mater. Sol. Cells* **2009**, *93*, 394.
[5] E. Bundgaard, O. Hagemann, M. Manceau, M. Jørgensen, F. C. Krebs, *Macromolecules* **2010**, *43*, 8115.
[6] M. Manceau, D. Angmo, M. Jørgensen, F. C. Krebs, *Org. Electron.* **2011**, *12*, 566.
[7] F. C. Krebs, J. Fyenbo, M. Jørgensen, *J. Mater. Chem.* **2010**, *20*, 8994.
[8] S. W. Heo, J. Y. Lee, H. J. Song, J. R. Ku, D. K. Moon, *Sol. Energy Mater. Sol. Cells* **2011**, *95*, 3041.
[9] S. W. Heo, K. W. Song, M. H. Choi, T. H. Sung, *Sol. Energy Mater. Sol. Cells* **2011**, *95*, 3564.
[10] C. E. Wu, S. Y. Chen, C. Cui, Y. J. Cheng, C. S. Hsu, Y. L. Wang, Y. Li, *Angew. Chem. Int. Ed.* **2011**, *50*, 9386.
[11] L. Huo, S. Zhang, X. Guo, F. Xu, Y. Li, J. Hou, *Angew. Chem. Int. Ed.* **2011**, *50*, 9697.
[12] Z. He, C. Zhong, X. Huang, W.-Y. Wong, H. Wu, L. Chen, S. Su, Y. Cao, *Adv. Mater.* **2011**, *23*, 4636.
[13] J. Y. Lee, W. S. Shin, J. R. Haw, D. K. Moon, *J. Mater. Chem.* **2009**, *19*, 4938.

[14] J. Y. Lee, S. W. Heo, H. Choi, Y. J. Kwon, J. R. Haw, D. K. Moon, *Sol. Energy Mater. Sol. Cells* **2009**, *93*, 1932.
[15] P. W. M. Blom, V. D. Mihailetchi, L. J. A. Koster, D. E. Markov, *Adv. Mater.* **2007**, *19*, 1551.
[16] Y. Wang, L. Yang, C. Yao, W. Qin, S. Yin, F. Zhang, *Sol. Energy Mater. Sol. Cells* **2011**, *95*, 1243.
[17] J. M. Yun, J. S. Yeo, J. Kim, H. G. Jeong, D. Y. Kim, Y. J. Noh, S. S. Kim, B. C. Ku, S. I. Na, *Adv. Mater.* **2011**, *23*, 4923.
[18] Y. Yao, J. Hou, Z. Xu, G. Li, Y. Yang, *Adv. Funct. Mater.* **2008**, *18*, 1783.
[19] P. Vanlaeke, A. Swinnen, I. Haeldermans, G. Vanhoyland, T. Aernouts, D. Cheyns, C. Deibel, J. D'Haen, P. Heremans, J. Poortmans, J. V. Manca, *Sol. Energy Mater. Sol. Cells* **2006**, *90*, 2150.
[20] J. K. Lee, W. L. Ma, C. J. Brabec, J. Yuen, J. S. Moon, J. Y. Kim, K. Lee, G. C. Bazan, A. J. Heeger, *J. Am. Chem. Soc.* **2008**, *130*, 3619.
[21] F. Padinger, R. S. Rittberger, N. S. Sariciftci, *Adv. Funct. Mater.* **2003**, *13*, 85.
[22] W. L. Ma, C. Y. Yang, X. Gong, K. Lee, A. J. Heeger, *Adv. Funct. Mater.* **2005**, *15*, 1617.
[23] G. Li, V. Shrotriya, J. S. Huang, Y. Yao, T. Moriarty, K. Emery, Y. Yang, *Nat. Mater.* **2005**, *4*, 864.
[24] F. Zhang, K. G. Jespersen, C. Bjorstrom, M. Svensson, M. R. Andersson, V. Sundstrom, K. Magnusson, E. Moons, A. Yartsev, O. Inganas, *Adv. Funct. Mater.* **2006**, *16*, 667.
[25] J. Peet, N. S. Cho, S. K. Lee, G. C. Bazan, *Macromolecules* **2008**, *41*, 8655.
[26] S. W. Heo, S. H. Kim, E. J. Lee, D. K. Moon, *Sol. Energy Mater. Sol. Cells* **2013**, *111*, 16.
[27] K. L. Woon, M. P. Aldred, P. Vlachos, G. H. Mehl, T. Stirner, S. M. Kelly, M. O'Neill, *Chem. Mater.* **2006**, *18*, 2311.
[28] N. Yilmaz Canli, S. Günes, A. Pivrikas, A. Fuchsbauer, D. Sinwel, N. S. Sariciftci, O. Yasa, B. Bilgin-Eran, *Sol. Energy Mater. Sol. Cells* **2010**, *94*, 1089.
[29] S. Jeong, S. H. Woo, H. K. Lyu, Y. S. Han, *Sol. Energy Mater. Sol. Cells* **2011**, *95*, 1908.
[30] Y.-M. Chang, L. Wang, *J. Phys. Chem. C* **2008**, *112*, 17716.
[31] S. W. Heo, I. S. Song, Y. S. Kim, D. K. Moon, *Sol. Energy Mater. Sol. Cells* **2012**, *101*, 295.